ECS Advances, 2022 **1** 030504

An Enhanced Battery Aging Model Based on a Detailed Diffusing Mechanism in the SEI Layer

Amirmasoud Lanjan[1] **and Seshasai Srinivasan**[1,2,z]

[1]*Department of Mechanical Engineering, McMaster University, Hamilton, ON, Canada*
[2]*W Booth School of Engineering Practice and Technology, McMaster University, Hamilton, ON, Canada*

The impetus for this study is the lack of a detailed knowledge on the formation mechanism of the solid electrolyte interface (SEI) layer and the diffusion mechanisms within this layer that impacts the predictive abilities of the current mathematical models. Specifically, most models continue to employ a constant value of diffusion coefficient along with several lumped fitting parameters, instead of a variable formulation that is dependent on the temperature and concentration of Li-ions, to characterize Li-ion batteries (LIBs). As a result, the current models fail in predicting the capacity fading accurately. In overcoming this gap, we have employed a previously proposed temperature and concentration-dependent diffusion equation to present a modified mathematical model that is capable of accurately predicting the capacity fading and SEI growth rate as a function of temperature, concentration, and time, with just two significantly simplified temperature dependent fitting parameters. Further, these parameters need to be adjusted only for new temperatures. Our enhanced model is validated with respect to the experimental data for different operational conditions, including open circuit condition with different initial state of charges (SOCs) as well as cycling with a constant current.
 [DOI: 10.1149/2754-2734/ac8e84]

Manuscript received August 22, 2022. Published September 9, 2022.

Nomenclature

Symbol	Unit	Description
a_{crd}	1	Proportionality factor
A	m^2	Electrode surface area
C	$\frac{mol}{m^3}$	Reactant concentration of SEI formation
C_{batt}	1	Relative capacity
D_i	$\frac{m^2}{s}$	Diffusion coefficient
$E_{eq,i}$	V	Equilibrium potential
f	1	Lumped fitting parameter
F	$\frac{C}{mol}$	Faraday's constant, 96 485
I_0	A	Exchange current
I_{1C}	A	1C charge/discharge current, 2.3
I_{kin}	A	Kinetic current
I_{lim}	A	Limiting current
I_{load}	A	Applied current on the battery
J	1	Lumped fitting parameter
H	1	Lumped fitting parameter
$Q_{batt,0}$	C	Initial battery capacity, 2.3
Q_{neg}	C	Charge stored in the negative electrode
Q_{SEI}	C	Charge lost to SEI forming reactions
R	$\frac{J}{molK}$	Molar gas constant, 8.3145
s	m	SEI layer thickness
T	k	Temperature
V	$\frac{m^3}{C}$	Coulombic volume for forming the SEI
x	1	Stoichiometric coefficient in Li_xC_6
α	1	Transfer coefficient
ϵ_i	1	Porosity
η_i	V	Over-potential
Φ_i	V	Potential of i phase
τ_i	1	Tortuosity

Index	Description
cov	Areas covered by an microporous SEI layer
crd	Areas where the SEI layer has cracked
ical	Intercalating reaction
neg	negative electrode
SEI	SEI layer or SEI layer forming reaction
s	Solid (Electrode) phase
l	Liquid (Electrolyte) phase

In the transportation sector, a high proportion of the emissions of greenhouse gases (GHG) (∼50%) and energy consumption (∼50%) are contributing significantly to environmental issues. Therefore, transport electrification is critical to address the current environmental issues, and has attracted a lot of political and social attention. This receives further impetus from the fact that a typical electric motor (EM) utilized in electric vehicles (EVs) has a significantly higher efficiency (>90%) than internal combustion engines (ICEs) (<15%). Still, one of the biggest barriers in adopting this transformation of the transport sector is the limited lifespan of Li-ion batteries (LIBs). In addition to the costs, LIBs' short lifetime will produce a lot of waste materials which is beginning to pose a new environmental problem. Therefore, extending a battery's lifespan is critical for transport electrification and mitigating environmental issues.

The main parts of LIBs, i.e., the electrolyte, the cathode, and the anode have been well investigated in recent years.[1–6] While these studies have improved the LIBs' performance parameters (e.g., capacity, power, voltage), precise aging mechanisms are still largely unknown. Moreover, even in the recent well-engineered LIBs, over 50% of capacity loss is due to the solid electrolyte interface (SEI) layer.[7–10]

The SEI layer was first observed and reported by Peled in 1979.[11] This layer is formed through some reduction and oxidation reactions on the electrode surface. When the cathode's potential is lower and/or the anode's potential is higher than the electrolyte's oxidation and/or reduction potentials, the electrolyte molecules are oxidized and/or reduced on the electrode surface, respectively. The products

[z]E-mail: ssriniv@mcmaster.ca

of these oxidation and reduction reactions will accumulate on the surface, forming the SEI layer.[7,12] These oxidation and reduction potentials of the electrolyte directly depend on the highest occupied molecular orbital (HOMO) and the lowest unoccupied molecular orbital (LUMO) energy level, respectively.[12,13] It must be noted that the operating conditions of a battery, such as the loaded voltage, current and temperature, affect these potential window. The SEI formation reactions decompose the electrolyte's molecules and consume active Li-ions resulting in a capacity loss.[14]

An intact and well-designed SEI layer reduces electron tunneling and electrolyte diffusion at the electrode-electrolyte interface. This further decreases the SEI formation and reduction reactions, and thereby the rate of capacity fading.[7] A typical SEI layer comprises the following: (I) An inorganic inner layer which is closer to the electrode interface and is only permeable for Li-ions. (II) An organic porous outer layer which is closer to the electrolyte interface and that allows the transport of electrolyte solvent molecules as well as Li-ions.[15,16] Therefore, characterizing and understanding the SEI layer transportation and formation mechanisms is the key to improving LIBs' durability.[17,18]

Since some of the SEI formation reactions occur at picosesond (ps) timescales, experimental investigations are very challenging. Therefore, multi-scale multi-physics modelling including Quantum Mechanics (QM) calculations, Molecular Dynamics (MD) simulations, and Macro-Scale mathematical modelling are often employed by researchers to understand the mechanisms at various time and length scales that cause the aging in LIBs, overcoming the constraints and limitations of the experimental methods.[19–24]

Christensen and Newman[25] developed a model to estimate the rate of SEI growth and irreversible capacity loss. However, due to the lack of information on the diffusion coefficient equation in the SEI layer, they assumed a constant diffusion coefficient of $5.0 \times 10^{-14}\left(\frac{m^2}{s}\right)$ for all the ions (Li^+ and PF_6^-) in every region. Thus, a lack of clarity on the diffusion mechanism in the SEI layer and the complexity of this structure results in the discrepancies between predictions from the mathematical models such as the ones by Christensen and Newman[25] and the actual aging behavior of LIBs. This claim is further supported by the work of Deng et al.[26] who have shown that the SEI formation is a diffusion-limited phenomenon which is governed by the value of the diffusion coefficient in this layer. Liu et al.[27] developed a model indicating a spatial dependence of the SEI layer formation in LIBs. They found that in a diffusion-limited system, the thickness of the SEI layer can increase from 4 nm to 20 nm (500%) if the diffusion coefficient in the SEI layer is doubled.[27] However, as with the other researchers,[27–32] with an insufficient understanding of the diffusion mechanisms, resulting in the lack of a temperature and concentration-dependent equation for the diffusion coefficient, they used the constant value proposed by Christensen and Newman.[25] In summary, to develop a good understanding of the aging mechanisms in a LIB, we need an accurate mathematical model to estimate LIBs' lifespan that accounts for the capacity fade due to the SEI growth rate.

In 2015, Ekström and Lindbergh[33] derived a macro-scale mathematical continuum model to estimate the effect of SEI layer formation on the aging of LIBs that use a graphite anode material. The model is a combination of kinetic and transport control systems and uses a constant diffusion coefficient. In their model, the authors proposed three lumped fitting parameters which are substituted in the Eqs. instead of variables such as a diffusion coefficient. Using these parameters improves the accuracy of the model with respect to the experimental data for a range of temperature and concentration values. However, the problem with these fitting parameters is that they need to be adjusted experimentally before we can employ the model. Further, the fitting parameters will vary with the material of the LIBs, prohibiting us from a computational exploration of new and novel materials in LIBs.

In our previous work,[14] we used a combination of QM calculations and MD simulations to prescribe a temperature and Li-ion concentration-dependent equation for the diffusion coefficient for every crystal structure in the inner part of the SEI layer. Subsequently, to accurately model the physics within the SEI layer, the macro-scale mathematical model was equipped with a single equation for the diffusion coefficient. Specifically, the diffusion coefficient equation in our previous work[14] was integrated into a popular macro-scale mathematical model (MSMM) from Ekström and Lindbergh[33] that is used in commercialized engineering software, i.e., Comsol Multiphysics, to investigate SEI growth and capacity fading. The results obtained from our proposed formulation are validated with respect to the experimental data and compared with the results obtained by using a model with constant diffusion coefficient to highlight the accuracy and impact of our new formulation. In other words, as the outcome of this work, a modified version of the Ekström and Lindbergh MSMM is proposed in which only two simplified fitting parameters are used, eliminating the most complicated parameter in the original model. Our revised formulation accounts for the effect of temperature and concentration on ageing. We use this model to study SEI growth and capacity fading as a function of time and initial SOC for a wide range of temperatures and concentrations.

Table I. The constants in Eq. 2 for the SEI components Li_2O and LiF.

	A_0	$D_0\left[\frac{m^2}{s}\right]$	R^2
Li_2O	4.07×10^{-2}	1.54×10^{-10}	0.98
LiF	1.128×10^{-1}	5.10×10^{-10}	0.96

The Theoretical Method and Computational Details

SEI components.—The inner Section of the SEI layer is made of three main components, namely, Li_2CO_3, LiF, and Li_2O.[13,16,34–36] Experimental and theoretical studies indicated that Li_2CO_3 is a component in the SEI layer, produced by a reaction of $CoCO_3$ and Li-ion in presence of the ethylene carbonate (EC).[37] Several studies[38,39] found that the thermodynamically unstable Li_2CO_3 will reduce to Li_2O and Li_2C_2. Li_2C_2 will further decompose to Li^+, C_2H_2, and C.[39] Consequently, Li_2CO_3 cannot be considered as a permanent component in a SEI layer's inner section.[37–39] Therefore, in this work, only LiF and Li_2O are assumed as the constant components in this part.

Diffusion equation.—Li-ion diffusion coefficient in the SEI layer (D_T) are calculated as Ref. 14:

$$D_T = \delta_{LiF}\, D_{LiF} + \delta_{Li_2O}\, D_{Li_2O}, \quad [1]$$

where δ_i and D_i is the surface area fraction and diffusion coefficient of component i, respectively. Further, the diffusion coefficient of each component can be calculated as a function of temperature and concentration as:

$$D_i(C, T) = D_0 \exp\left(\frac{-A_0\, EB(C)}{k_b\, T}\right), \quad [2]$$

where D_0 and A_0 are SEI component dependent constants that are reported in Table I.[14] In the above equation, EB is the energy barrier which can be calculated as a function of concentration via:

$$EB(C_{Li^+}) = a_2 C_{Li^+}^2 + a_1 C_{Li^+}^1 + a_0, \quad [3]$$

where the SEI component dependent constants a_0, a_1, and a_2 are summarized in Table II.[14]

Table II. The coefficients of the second-degree polynomial $EB = a_2 C_{Li^+}^2 + a_1 C_{Li^+}^1 + a_0$ (Eq. 3) for Li_2O and LiF.

	a_0 [eV]	a_1 [eV]	a_2 [eV]	R^2
Li_2O	3.9488	−8.9294	12.0460	0.96
LiF	1.9886	−2.5607	3.5237	0.93

Table III. Employed parameters for the modified MSMM aging model introduced in this work.

Parameter	25 °C	45 °C
f	4.5×10^6	7.0×10^5
H	6.8	3.9

Since it would be difficult to directly measure the fraction of the surface area of different components in the SEI layer, δ_i can be obtained as follow:

$$\omega_i = \frac{m_i}{m_{Li_2O} + m_{LiF}}, \quad [4]$$

$$\delta_{Li_2O} = \frac{\omega_{Li_2O}}{\omega_{Li_2O} + \frac{\rho_{Li_2O}}{\rho_{LiF}}\omega_{LiF}} \text{ and}$$
$$\delta_{LiF} = \frac{\omega_{LiF}}{\omega_{LiF} + \frac{\rho_{LiF}}{\rho_{Li_2O}}\omega_{Li_2O}}, \quad [5]$$

where m, L, ω and ρ, are mass, thickness, mass fraction, and density of the material i, either LiF or Li_2O, in the SEI layer, respectively.

A mathematical model for aging.—In this work, we present a modified version of the Ekström and Lindbergh[33] model. Specifically, the enhanced model uses only two simplified fitting parameters and uses a temperature and Li-ion concentration-dependent diffusion coefficient equation proposed in our previous work.[14] The resulting model uses the information on SEI growth rate more precisely to estimate the aging of the battery and helps enhance the accuracy of the model. We establish the superior performance of this enhanced model by comparing it with the original model that uses three complex fitting parameters instead of a diffusion coefficient value. Specifically, we present a zero-dimensional model which uses a galvanostatic mode in battery cycling and therefore does not require the definition of a positive electrode or the electrolyte.

In this model, the accumulated charge (Q_{SEI} (C)), which is lost in LIBs due to the SEI formation reactions, is calculated as follows:[33]

$$\frac{dQ_{SEI}}{dt} = -I_{SEI}, \quad [6]$$

where I_{SEI} is the sum of the current distribution passing through the surfaces that are fully covered by the intact or cracked SEI layer. The derivation of I_{SEI}, outlined in the Appendix, yields the following expression:

$$I_{SEI} = -(1 + HK_{crd})\frac{JI_{1C}}{exp\left(\frac{\alpha F \eta_{SEI}}{RT}\right) + \frac{fJQ_{SEI}}{I_{1C}}}, \quad [7]$$

where I_{1C} are the currents through the cracked parts and 1 C-rate charging current, respectively. Additionally, J, H, and f are three lumped fitting parameters to compensate for the lack of knowledge regarding SEI and aging phenomena which need to be fitted for each new battery cell and/or operational condition. In the original Ekström and Lindbergh model,[33] these fitting parameters are defined as:

Table IV. The constants in Eq. 12.

$f_0\left[\frac{1}{K}\right]$	f_1	$H_0\left[\frac{1}{K}\right]$	H_1
-1.9×10^5	6.1×10^7	−0.14	49.5

$$J = \frac{\epsilon_{cov} I_0}{I_{1C}}, \quad [8]$$

$$f = \frac{\tau_{cov} V I_{1C}^2}{\epsilon_{cov}(1 - \epsilon_{cov}) CDFA^2}, \quad [9]$$

$$H = \frac{a_{crd}}{\epsilon_{cov}}. \quad [10]$$

The parameters in these Eqs. are described in the nomenclature. A detailed description of the derivation of the Eqs. in this model are presented in the Appendix.

As mentioned earlier, the SEI layer is made of different materials and crystal structures, namely, Li_2O and LiF. Also, different particles diffuse through these crystal structures including electrolyte solvent molecules and Li-ions with different sizes and charge values. Therefore, the diffusion coefficient values would vary widely for different particles in these various structures, and will be impacted by the operating temperatures and concentrations. Due to the lack of data for the complex diffusion and reaction mechanisms, J, f, and H (Eqs. 8–10) are employed to increase the accuracy of the model and reduce the deviation from experimental data.

Since the accumulation of Li-ions increases the charge profile gradient in the SEI layer, it raises the electron leakage, increasing I_0. On the other hand, reducing the diffusion coefficient increases the Li-ions gradient. This clearly indicates that I_0 is inversely proportional to D_T. Consequently, I_0 can be reversely proportional to the D_T. Therefore, in this work, modifying E. 8, we employed the following expression for J that uses a material constant (J_0) and D_T.:

$$J = \frac{J_0}{D_T} \quad [11]$$

In the above equation, D_T is the expression given in Eq. 1. Also, J_0 is $1.49 \times 10^{-16}\left[\frac{m^2}{s}\right]$, a material constant that is dependent on the solvent molecules. Thus, with the introduction of this equation, the first lumped fitting parameter (J) is no longer required. In other words, we have eliminated the fitting parameter J in the modified model and reduced the number of lumped fitting parameters to two.

Simplified expressions for the remaining two fitting parameters, i.e., f and H, were developed as follows: We obtained experimental data from the literature for the following three aging conditions at two different temperatures (25 °C and 45 °C):[33,40]

1. charge/discharge cycling with 1 C-rate load current
2. open circuit at 50% SOC
3. open circuit at 100% SOC

The Ekström and Lindbergh model with the updated expression for J (Eq. 11) was applied to these data and the model was tuned for the values of f and H to reflect the highest possible accuracy. The tuned values of these parameters are summarized in Table III. Finally, with these tuned values of f and H for a temperature range of [25 °C, 45 °C], a linear profile of these parameters as a function of temperature was defined as follows:

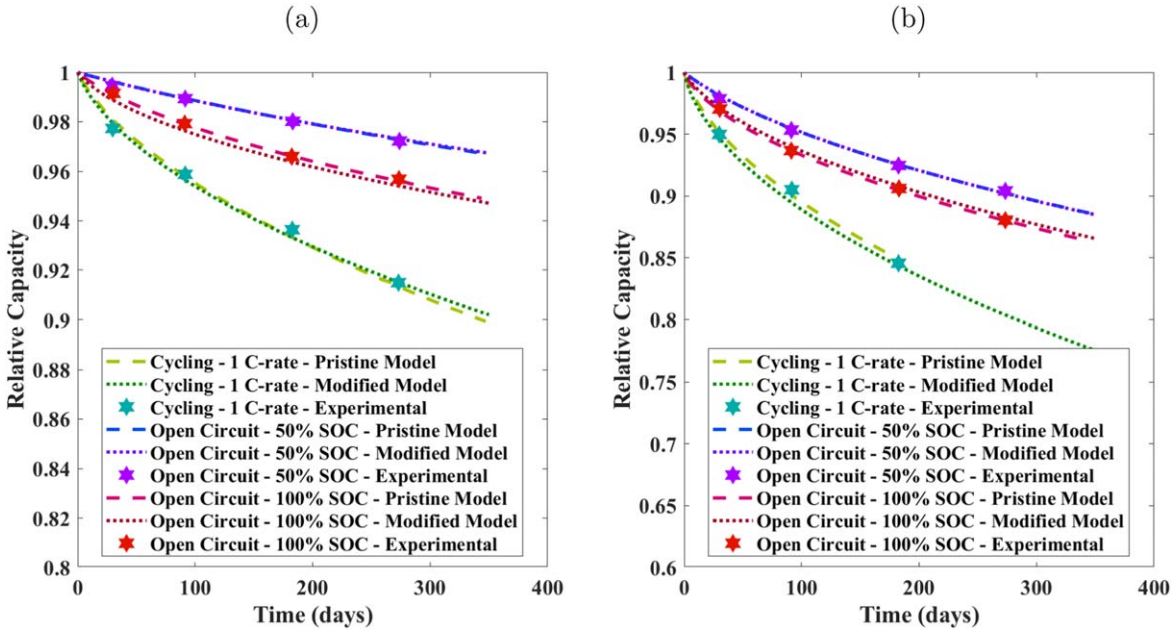

Figure 1. Relative capacity versus time for a duration of 350 days: Markers, dashed, and dotted lines are for the experimental data,[33] pristine model and the modified model, respectively at (a) 25 °C and (b) 45 °C. At each temperature, the relative capacity has been obtained for open circuit condition with 50% and 100% initial capacity as well as for the cycling operation with I_{1C} (1 C-rate) current.

$$f(T) = f_0\, T + f_1, \qquad [12]$$

$$H(T) = H_0\, T + H_1. \qquad [13]$$

where f_0 and H_0 are reported in Table IV.

Thus, the modified Ekström and Lindbergh model presented in this work uses simpler revised expressions for J, f and H, that collectively account for the temperature and concentration of the Li-ions.

While this diffusion coefficient equation (Eq. 1) employs the same formulation for all diffusing particles, contributing to the deviation from experimental results, it adequately accounts for the effects of different concentrations, temperatures and crystal structures on diffusion coefficient and SEI formation. In the ensuing section, we demonstrate that our modified model is able to predict the experimental data with high accuracy, justifying the new formulation that limits the number of fitting parameters to two.

Additionally, accounting for the capacity fade due to the loss of Li-ions during the SEI formation, the Relative capacity (RC) can be calculated as:

$$\mathrm{RC} = \frac{Q_{batt,0} - Q_{SEI}}{Q_{batt,0}}, \qquad [14]$$

where $Q_{batt,0}$ is the initial battery capacity. Moreover, the SEI thickness can be estimated as:

Table V. R^2 values of the estimated relative capacity using the pristine and the modified MSMM models with respect to the experimental data.

Temperature	Operational condition	Pristine	Modified
25 °C	Open Circuit - 50% SOC	0.99	0.99
25 °C	Open Circuit - 100% SOC	0.99	0.97
25 °C	Cycling - 1 C-rate	0.99	0.98
45 °C	Open Circuit - 50% SOC	0.99	0.99
45 °C	Open Circuit - 100% SOC	0.99	0.98
45 °C	Cycling - 1 C-rate	0.99	0.98

$$s = \frac{Q_{SEI}\, V}{(1 - \epsilon_{cov})A}. \qquad [15]$$

In our calculations, the initial charge accumulation (Q_{SEI}) is set to zero at $t = 0$, and the initial relative capacity (RC) is 100%. All the indexes and symbols used in this model are defined in the nomenclature. The relative capacity during 400 days at the three different aging conditions described earlier, each at two different temperatures (25 °C and 45 °C), were evaluated employing the pristine and modified Ekström and Lindbergh model presented in this work, and the results are compared with the experimental data.

Results and Discussion

We investigated capacity fading as a function of time at two different temperatures using the modified MSMM model that is equipped with a temperature and concentration-dependent diffusion equation (Eq. 1) for D_T. As mentioned earlier, the experimental data from the three different battery aging conditions, each at two different temperatures, were used for validating the model.

The results obtained from this investigation are presented in Fig. 1. As seen in this figure, the results from the pristine model and the modified MSMM model that use three and two lumped fitting parameters, respectively. To facilitate the comparison of the models, experimental data is also included for all the simulated conditions. The results show that both models, i.e., the pristine and the modified MSMM model, produce results that are in good agreement with the experimental data.

The R^2 for the pristine and modified MSMM model with respect to the experimental data is summarized in Table V. Therefore, substituting the diffusion coefficient in Eq. 11 and calculating the value of J directly for a specific temperature and operating condition not only reduces the number of required parameters, revealing the effects of the diffusion coefficient in the SEI layer on the capacity fading, but also increase the accuracy of the model for a wide range of SOC values.

As seen in Table V, the accuracy of the pristine model is higher than 99% which is either equal to or marginally better than the modified model. However, the pristine model needs re-tuning of the

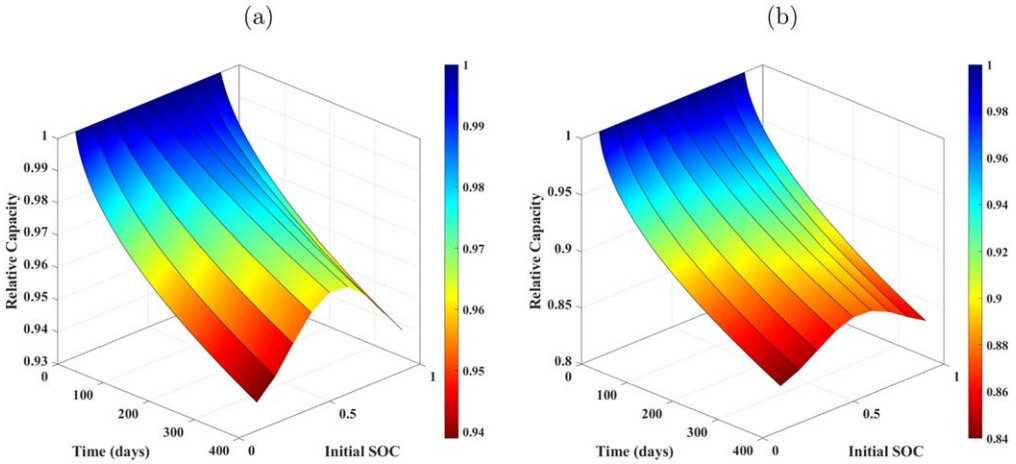

Figure 2. Relative capacity for different operating conditions for a duration of 350 days in (a) 25 °C and (b) 45 °C.

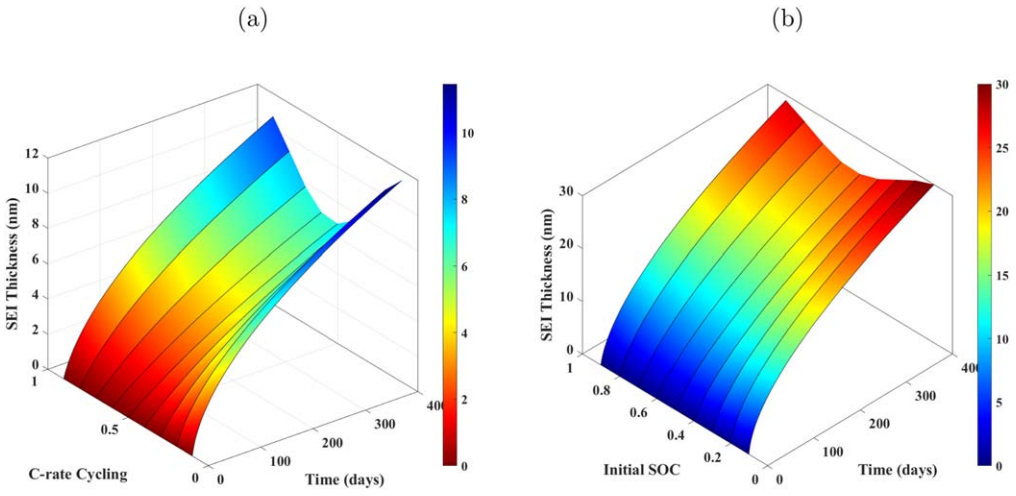

Figure 3. The SEI thickness for different operating conditions for a duration of 350 days in (a) 25 °C and (b) 45 °C.

three fitting parameters for each SOC and employing the same values of the parameters for a wide range of SOC will reduce the model's accuracy to lower than 10%. On the other hand, the modified model does not require any parameter adjustment for the entire range of SOCs (from 0% to 100%). In this model, two fitting parameters (f and H) are a function of temperature and instead of the third parameter (J), we directly employ the diffusion coefficient, collectively accounting for the impact of other variables. By employing such fixed parameters in the modified model for a variety of operating conditions, the accuracy is still as high as 98% (c.f. Table V).

The relative capacity was also calculated for a wide range of initial SOC and two temperatures, and the results are shown in Fig. 2. As seen in this figure, as the temperature increases, the capacity fading rate increases significantly. This is while the relation between SOC and capacity fading is not linear and follows a quadratic trend in a way that the highest capacity fading occurs at the highest as well as the lowest SOC. Also, the slowest aging rate observed was at around 50% SOC. These results are in good agreement with the experimental data in the literature.[40]

The SEI thickness as a function of time and initial SOC is shown in Fig. 3. It is seen that the SEI growth is highly sensitive to temperature and it increases from around 11 nm to 30 nm when the temperature increases from 25 °C to 45 °C. Also, SEI thickness is more sensitive to the initial SOC in lower temperatures and grows from 8 nm to 11 nm as we move far from 50% initial SOC. Overall, the range of the SEI thickness and its relation with the initial SOC and temperature are in good agreement with the experimental data in the literature.[40]

Further Investigation

We have presented the validity of an enhanced model that uses fewer fitting parameters, with respect to experimental data from diverse operating conditions. However, in the Macro-scale simulations, we have assumed the same diffusion behavior through the entire SEI layer for all particles. This approximation is one of the probable reasons for the deviations of the model predictions from the experimental data. On the other hand, the outer Section of SEI constitutes a wide variety of components and is directly dependent on the electrolyte of LIBs. So, the diffusion equation will vary depending upon the type of electrolyte used. Hence, further investigations are required to reveal additional details on the diffusion mechanisms in the SEI layer and provide a diffusion equation which includes the effects of charge and size of different particles, and the outer Section of the SEI layer, on the diffusion coefficient and SEI formation reactions.

Conclusions

SEI formation reactions consume active Li-ions and electrolyte molecules in the LIBs, resulting in a capacity fade. Being directly dictated by the SEI growth rate, the capacity fading rate has the highest value at $t = 0$ and will decrease with time, and is sensitive to LIB's operating temperature. Overall, capacity fading and SEI

growth rate are governed by the temperature and concentration-dependent diffusion processes inside the SEI layer.

Incorporating this into the macro-scale mathematical model, we have presented an enhanced version of the Ekström and Lindbergh[33] model using just two modified lumped fitting parameters as well as the equation of D_T (Eq. 1)[14] which are adequately capable of predicting the decay in the relative capacity of a LIB as a function of time. This is validated with respect to the experimental data at two different temperatures during the following aging conditions: (I) charge/discharging cycling with 1 C-rate load current, (II) open circuit condition at 50% SOC, and (III) open circuit condition at 100% SOC (c.f. Fig. 1a). Further, the enhanced model is also capable of predicting the SEI growth rate as a function of temperature and Li-ion concentration.

It must be noted that not only does the modified MSMM model have just two fitting parameters with simpler temperature dependent formulations but it can also accurately predict the capacity fading and the SEI growth rate for different operational condition and initial SOCs with fixed parameters. In other words, the fitting parameters must be evaluated only for each different operational temperature in the modified model.

Appendix: Derivation of I_{SEI}

The total current through a SEI layer can be written as:

$$I_{SEI} = I_{cov} + I_{crd}, \qquad [A\cdot1]$$

where I_{cov} and I_{crd} are the currents through the covered and cracked parts, respectively.

Further, $I_{cov\ (or\ crd)}$ can be written based on a first-order mass transfer restricting current through a Nernst boundary layer as:

$$I_{cov\ (or\ crd)} = \frac{I_{kin,cov\ (or\ crd)}}{1 + \frac{I_{kin,cov\ (or\ crd)}}{I_{lim.cov\ (or\ crd)}}}. \qquad [A\cdot2]$$

In this equation, $I_{kin.cov(or\ crd)}$ (A) is the kinetic current, and I_{lim} is the highest current of the SEI formation, restricted by the mass transport. These currents can be calculated as:

$$I_{kin.cov\ (or\ crd)} = -\epsilon_{cov\ (or\ crd)} I_0\ exp\left(-\frac{\alpha\eta_{SEI}F}{RT}\right), \qquad [A\cdot3]$$

where I_0 and η_{SEI} are the exchange current and the over potential of the SEI formation reaction, respectively. All other symbols and notations are defined in the nomenclature section. Also, ϵ_{crd} and ϵ_{cov} are calculated as:

$$\epsilon_{crd} = a_{crd} K_{crd}, \qquad [A\cdot4]$$

$$\epsilon_{cov} = 1 - \epsilon_{crd}, \qquad [A\cdot5]$$

where K_{crd} and a_{crd} are the expansion factor and a dimensionless proportionality factor, respectively. Further, for K_{crd}, we have:

$$K_{crd} = \begin{cases} -2\frac{I_{ical}}{I_{1C}} & I_{ical} < 0 \text{ and } x < 0.3 \\ 0 & I_{ical} < 0 \text{ and } 0.3 \leqslant x \leqslant 0.7 \\ -\frac{I_{ical}}{I_{1C}} & I_{ical} < 0 \text{ and } 0.7 \leqslant x \\ 0 & I_{ical} \geqslant 0 \end{cases} \qquad [A\cdot6]$$

The over potential of the SEI formation reaction can be calculated by setting the SEI reaction equilibrium potential ($E_{qe,SEI}$) to zero and evaluating the difference between the electrode potential (Φ_s) and electrolyte potential (Φ_l) as follows:

$$\eta_{SEI} = \Phi_s - \Phi_l - E_{qe,SEI}. \qquad [A\cdot7]$$

It must be noted that the liquid phase potential is directly related to the intercalation reaction's equilibrium potential ($E_{qe,ical}$) and the corresponding over potential, η_{ical}, and can be expressed as:

$$\Phi_l = -(E_{qe,ical} + \eta_{ical}). \qquad [A\cdot8]$$

By inverting the Butler-Volmer equation, the relationship between the over potential and the intercalation current can be written as:

$$\eta_{ical} = \frac{RT}{0.5F}\text{arcsinh}\left(\frac{I_{ical}}{2k_{ical}I_{1C}((1-x)x)^{0.5}}\right), \qquad [A\cdot9]$$

where x and I_{ical} are the SOC and intercalation current of the anode, respectively. I_{1C} is the battery's nominal 1C charge, and k_{ical} is the proportionality constant chosen to render the over potential. In the Nernst boundary layer, the limiting current density and the accumulated SEI layer thickness are inversely related:

$$I_{lim.cov\ (or\ crd)} = -\frac{\epsilon_{cov\ (or\ crd)} CD_{cov(orcord)} FA}{s}, \qquad [A\cdot10]$$

where C, F, and A are the concentration, Faraday's constant, and electrode surface area, respectively. $D_{cov(orcord)}$ is inversely related to the tortuosity of the layer as:

$$D_{cov(orcord)} = \frac{D_T}{\tau_{cov}}. \qquad [A\cdot11]$$

Finally, to minimize the error and improve the accuracy of the model, Ekström and Lindbergh[33] proposed the following three lumped fitting parameters as:

$$J = \frac{\epsilon_{cov} I_0}{I_{1C}}, \qquad [A\cdot12]$$

$$f = \frac{\tau_{cov} V I_{1C}^2}{\epsilon_{cov}(1-\epsilon_{cov}) CDFA^2}, \qquad [A\cdot13]$$

$$H = \frac{a_{crd}}{\epsilon_{cov}}. \qquad [A\cdot14]$$

ORCID

Amirmasoud Lanjan https://orcid.org/0000-0003-1993-3866
Seshasai Srinivasan https://orcid.org/0000-0002-3765-3772

References

1. R. Tyagi, A. Lanjan, and S. Srinivasan, "Co-doping strategies to improve the electrochemical properties of LixMn2O4 cathodes for li-ion batteries." *ChemElectroChem*, **9**, e202101626 (2022).
2. Z. Moradi, A. Lanjan, and S. Srinivasan, "Enhancement of electrochemical properties of lithium rich li2ruo3 cathode material." *J. Electrochem. Soc.*, **167**, 110537 (2020).
3. A. Mace, S. Barthel, and B. Smit, "Automated multiscale approach to predict self-diffusion from a potential energy field." *J. Chem. Theory Comput.*, **15**, 2127 (2019).
4. N. Prasetyo, P. H. Hunenberger, and T. S. Hofer, "Single-ion thermodynamics from first principles: Calculation of the absolute hydration free energy and single-electrode potential of aqueous Li+ using ab initio quantum mechanical/molecular mechanical molecular dynamics simulations." *J. Chem. Theory Comput.*, **14**, 6443 (2018).
5. P. Ganesh, J. Kim, C. Park, M. Yoon, F. A. Reboredo, and P. R. Kent, "Binding and diffusion of lithium in graphite: quantum monte carlo benchmarks and validation of van der Waals density functional methods." *J. Chem. Theory Comput.*, **10**, 5318 (2014).
6. B. Wang, S. L. Li, and D. G. Truhlar, "Modeling the partial atomic charges in inorganometallic molecules and solids and charge redistribution in lithium-ion cathodes." *J. Chem. Theory Comput.*, **10**, 5640 (2014).
7. A. Wang, S. Kadam, H. Li, S. Shi, and Y. Qi, "Review on modeling of the anode solid electrolyte interphase (sei) for lithium-ion batteries." *NPJ Comput. Mater.*, **4**, 1 (2018).

8. P. Novák, F. Joho, R. Imhof, J. C. Panitz, and O. Haas, "In situ investigation of the interaction between graphite and electrolyte solutions." *J. Power Sources*, **81–82**, 212 (1999).
9. A. Naji, J. Ghanbaja, B. Humbert, P. Willmann, and D. Billaud, "Electroreduction of graphite in liclo4-ethylene carbonate electrolyte. characterization of the passivating layer by transmission electron microscopy and fourier-transform infrared spectroscopy." *J. Power Sources*, **63**, 33 (1996).
10. R. Fong, U. von Sacken, and J. R. Dahn, "Studies of lithium intercalation into carbons using nonaqueous electrochemical cells." *J. Electrochem. Soc.*, **137**, 2009 (1990).
11. E. Peled, "The electrochemical behavior of alkali and alkaline earth metals in nonaqueous battery systems—the solid electrolyte interphase model." *J. Electrochem. Soc.*, **126**, 2047 (1979).
12. K. Xu, "Nonaqueous liquid electrolytes for lithium-based rechargeable batteries." *Chem. Rev.*, **104**, 4303 (2004).
13. K. Xu, "Electrolytes and interphases in Li-Ion batteries and beyond." *Chem. Rev.*, **114**, 11503 (2014).
14. A. Lanjan, Z. Moradi, and S. Srinivasan, "Multiscale investigation of the diffusion mechanism within the solid-electrolyte interface layer: coupling quantum mechanics, molecular dynamics, and macroscale mathematical modeling." *ACS Appl. Mater. Interfaces*, **13**, 42220 (2021).
15. A. V. Cresce, S. M. Russell, D. R. Baker, K. J. Gaskell, and K. Xu, "In situ and quantitative characterization of solid electrolyte interphases." *Nano Lett.*, **14**, 1405 (2014).
16. S. Shi, P. Lu, Z. Liu, Y. Qi, L. G. Hector, H. Li, and S. J. Harris, "Direct Calculation of Li-ion Transport in the Solid Electrolyte Interphase." *JACS*, **134**, 15476 (2012).
17. F. Dinkelacker, P. Marzak, J. Yun, Y. Liang, and A. S. Bandarenka, "Multistage mechanism of lithium intercalation into graphite anodes in the presence of the solid electrolyte interface." *ACS Appl. Mater. Interfaces*, **10**, 14063 (2018).
18. D. Zheng, X.-Q. Yang, and D. Qu, "Stability of the solid electrolyte interface on the li electrode in li-s batteries." *ACS Appl. Mater. Interfaces*, **8**, 10360 (2016).
19. A. Lanjan, B. Ghalami Choobar, and S. Amjad-Iranagh, "First principle study on the application of crystalline cathodes $Li_2Mn_{0.5}TM_{0.5}O_3$ for promoting the performance of lithium-ion batteries." *Comput. Mater. Sci.*, **173**, 109417 (2020).
20. A. Lanjan, B. Ghalami Choobar, and S. Amjad-Iranagh, "Promoting lithium-ion battery performance by application of crystalline cathodes $Li_xMn_{1-z}Fe_zPO_4$." *J. Solid State Electrochem.*, **24**, 157 (2020).
21. Z. Moradi, A. Lanjan, and S. Srinivasan, "Multiscale investigation into the co-doping strategy on the electrochemical properties of Li_2RuO_3 cathodes for li-ion batteries." *ChemElectroChem*, **8**, 112 (2021).
22. Y. S. Meng and M. E. Arroyo-de Dompablo, "First principles computational materials design for energy storage materials in lithium ion batteries." *Energy Environ. Sci.*, **2**, 589 (2009).
23. D. E. Galvez-Aranda, V. Ponce, and J. M. Seminario, "Molecular dynamics simulations of the first charge of a li-ionsi-anode nanobattery." *J. Mol. Model.*, **23**, 1 (2017).
24. D. Grazioli, M. Magri, and A. Salvadori, "Computational modeling of li-ion batteries." *Computational Mechanics 2016 58:6*, **58**, 889 (2016).
25. J. Christensen and J. Newman, "A Mathematical Model for the Lithium-Ion Negative Electrode Solid Electrolyte Interphase." *Proceedings—Electrochemical Society*, **20**, 85 (2003).
26. J. Deng, G. J. Wagner, and R. P. Muller, "Phase field modeling of solid electrolyte interface formation in lithium ion batteries." *J. Electrochem. Soc.*, **160**, A487 (2013).
27. L. Liu, J. Park, X. Lin, A. M. Sastry, W. Lu, and A. Thermal-Electrochemical, "Model that gives spatial-dependent growth of solid electrolyte interphase in a li-ion battery." *J. Power Sources*, **268**, 482 (2014).
28. X. Huang, S. Ke, H. Lv, and Y. Liu, "A dynamic capacity fading model with thermal evolution considering variable electrode thickness for lithium-ion batteries." *Ionics*, **24**, 3439 (2018).
29. A. M. Colclasure, K. A. Smith, and R. J. Kee, "Modeling Detailed Chemistry and Transport for Solid-Electrolyte-Interface (SEI) Films in Li-Ion Batteries." *Electrochim. Acta*, **58**, 33 (2011).
30. G. K. Prasad and C. D. Rahn, "Model based identification of aging parameters in lithium ion batteries." *J. Power Sources*, **232**, 79 (2013).
31. S. Phul, A. Deshpande, and B. Krishnamurthy, "A mathematical model to study the effect of potential drop across the sei layer on the capacity fading of a lithium ion battery." *Electrochim. Acta*, **164**, 281 (2015).
32. B. Horstmann, F. Single, and A. Latz, "Review on multi-scale models of solid-electrolyte interphase formation." *Current Opinion in Electrochemistry*, **13**, 61 (2019).
33. H. Ekström and G. Lindbergh, "A model for predicting capacity fade due to SEI formation in a commercial graphite/LiFePO4Cell." *J. Electrochem. Soc.*, **162**, A1003 (2015).
34. E. Peled, D. Golodnitsky, and G. Ardel, "Advanced model for solid electrolyte interphase electrodes in liquid and polymer electrolytes." *J. Electrochem. Soc.*, **144**, L208 (1997).
35. V. A. Agubra and J. W. Fergus, "The formation and stability of the solid electrolyte interface on the graphite anode." *J. Power Sources*, **268**, 153 (2014).
36. D. Aurbach, B. Markovsky, M. D. Levi, E. Levi, A. Schechter, M. Moshkovich, and Y. Cohen, "New insights into the interactions between electrode materials and electrolyte solutions for advanced nonaqueous batteries." *J. Power Sources*, **81–82**, 95 (1999).
37. K. Leung, F. Soto, K. Hankins, P. B. Balbuena, and K. L. Harrison, "Stability of solid electrolyte interphase components on lithium metal and reactive anode material surfaces." *J. Phys. Chem. C*, **120**, 6302 (2016).
38. N. Tian, C. Hua, Z. Wang, and L. Chen, "Reversible reduction of Li_2CO_3." *J. Mater. Chem. A*, **3**, 14173 (2015).
39. E. J. McShane, A. M. Colclasure, D. E. Brown, Z. M. Konz, K. Smith, and B. D. McCloskey, "Quantification of inactive lithium and solid-electrolyte interphase species on graphite electrodes after fast charging." *ACS Energy Letters*, **5**, 2045 (2020).
40. M. Safari and C. Delacourt, "Aging of a commercial graphite/LiFePO4 cell." *J. Electrochem. Soc.*, **158**, A1123 (2011).